Diffraction from disordered vicinal surfaces with alternating terraces

Joachim Wollschläger
Fachbereich Physik, Universität Osnabrück, Barbarastrasse 7, D-49069 Osnabrück, Germany

Christoph Tegenkamp
Institut für Festkörperphysik, Leibniz Universität Hannover, Appelstrasse 2, D-30167 Hannover, Germany
(Received 15 March 2007; revised manuscript received 13 May 2007; published 29 June 2007)

Vicinal surfaces with terraces of alternating stress develop inhomogeneous distributions of terrace sizes which sometimes leads even to the formation of double steps. Both vicinal Si(001) and vicinal Ge(001) are typical examples for this behavior. However, vicinal surfaces of some alloys show this effect, too. It is well established that *average* terrace sizes can be evaluated from the splitting of peaks in surface sensitive diffraction experiments. More parameters, however, are necessary to obtain an improved characterization of the morphology of the vicinal surface. Therefore, we present a detailed analysis of diffraction patterns from alternating vicinal surfaces to extract more statistical data, e.g., standard deviations of the terrace size distributions, step rms widths, step correlation lengths, and kink densities. This analysis considers both profiles of (split) diffraction peaks and the profile of the diffuse scattering. In addition, the diffraction analysis is applied to vicinal Ge(001) to characterize the morphology in full detail.

DOI: 10.1103/PhysRevB.75.245439 PACS number(s): 61.14.Dc, 61.14.Hg, 68.35.Ct, 68.47.Fg

I. INTRODUCTION

Stepped surfaces are of special interest in both fields of crystal growth and catalysis. Burton *et al.* already emphasized the enormous importance of atomic steps for the growth of crystals in their fundamental paper in the early 1950s.[1] They pointed out that atomic steps offer ideal sites for the accommodation of single atoms so that the nucleation barrier, which exists on singular surfaces, is bypassed. Therefore, vicinal surfaces are often used if films of homogeneous thickness have to be formed (see Refs. 2 and 3 for reviews). Atomic steps and kinks are also preferred sites of adsorption, chemical reaction, and catalysis due to their higher coordination compared to sites on terraces.[4]

Experimental techniques such as scanning probe microscopy and surface diffraction are well developed to characterize vicinal surfaces with equivalent terraces (homogeneous surfaces). In this field, significant attention has especially been paid to the transition from well ordered vicinal surfaces with long range order of atomic steps to a rough state where vicinal surfaces lose long range order (see the review by Lapujoulade[5] and the cited literature therein).

The just mentioned vicinal surfaces with equivalent terraces will be called *homogeneous* vicinal surfaces in the following. In contrast to these surfaces, some vicinal surfaces of semiconductors, e.g., Si(001) and Ge(001), typically show inequivalent terraces due to rotated surface reconstructions, where the atomic steps are identical to the domain boundaries. Vicinal surfaces of some alloys also exhibit inequivalent terraces due to the different chemical compositions (see Refs. 6 and 7 and the cited literature therein). Therefore, these surfaces will be called *inhomogeneous*.

For both vicinal Si(001) surfaces and vicinal Ge(001) surfaces with miscut toward the $\langle 110 \rangle$ direction, the different alignments of dimer rows parallel or perpendicular to atomic steps, in combination with the internal stress due to dimerization, lead to an anisotropic interaction between steps (compressive and tensile stress, see reviews by Zandvliet[8,9]) while vicinal Si(001) surfaces with miscut toward the $\langle \bar{1}10 \rangle$ direction tend to the formation of facets. Therefore, there exist A and B terraces of inequivalent size for the first type of vicinal surfaces. The different structures of S_A and S_B steps yield additional energy contributions. Depending on the angle of miscut, it has been reported that these vicinal surfaces undergo a transition to vicinal surfaces with pure D_B double steps. First, the formation of D_B double steps has been reported by Wierenga *et al.* from experiments for both Si(001) and Ge(001) by scanning tunneling microscopy (STM).[10] Alerhand *et al.*[11,12] explained the creation of double steps as first order transition depending on the angle of miscut (and temperature). Later, Bartelt *et al.*[13] pointed out that there exists a range of coexistence between single and double steps. The critical angle of miscut is approximately 4° and 6° for Si(001) and Ge(001), respectively.[9]

On the one hand, step pairing has been reported for alloys such as $Cu_{83}Pd_{17}$ and Cu_3Au, too, which have been studied by STM, surface x-ray diffraction (SXRD), and He atom scattering.[6,7] On the other hand, some vicinal metal surfaces, e.g., W(430), form double steps at *high* temperatures as proven by electron diffraction by Dey *et al.*[14] This effect has been attributed to a lower energy for the formation of kinks for double height steps compared to single height steps.

For Si(001) and Ge(001), STM investigations additionally show that S_A steps and S_B steps have very different morphologies. While S_A steps are very straight with the formation of only very few kinks, S_B steps are rough and many kinks are formed. This effect can be attributed to the different stiffnesses of both S_A steps and S_B steps. It has recently been discussed how alternating stiffness of steps influences the terrace size distribution.[15]

The repulsive interaction between steps, which stabilizes vicinal surfaces, can be suppressed by adsorbates. Therefore, step bunches and facets can be formed after adsorption.[16,17] Here, metal adsorbates are of special importance for Si(001) (see Ref. 17 and literature cited herein).

As pointed out for vicinal surfaces of metals by Giesen,[18] it may be difficult to characterize the statistics of atomic steps (kink density, rms width, correlation length) by STM if atomic processes at steps as attachment or detachment of atoms from kinks are very fast compared to the time of recording STM micrographs. STM micrographs show frizzy steps under these circumstances. Therefore, diffraction experiments seem to be better suited to characterize the statistical behavior of vicinal surfaces under these aspects.

The splitting of peaks, which are singular peaks for nonvicinal singular surfaces, into two components has been reported in early low energy electron diffraction (LEED) studies on vicinal surfaces of $UO_2(111)$ by Ellis and Schwoebel[19] and Ge(111) by Henzler[20] in the late 1960s. The Ewald construction for diffraction from perfect vicinal surfaces has been described in Refs. 21 and 22. The authors analyzed the data with respect to the terrace size and the step height. Early LEED studies on vicinal Si(001) (Refs. 23–25) already clarified the existence of double steps for large angles of miscut prior to the STM studies mentioned above.

This analysis assumed perfect vicinal surfaces with identical terrace sizes, straight steps, and identical step heights. This assumption, however, is only valid if the surface steps repulsively interact and for very low temperature without any significant entropic contributions. It is clear that, at least, meandering of steps and variations of terraces sizes become significant at higher temperatures (see the roughening transition for homogeneous vicinal surfaces mentioned above).

In a former paper, we developed a detailed statistical analysis of the diffraction pattern with respect to rms width, correlation length, and kink density of meandering noncolliding steps for homogeneous vicinal surfaces.[26] We cross-checked the theory with results from kinetic Monte Carlo simulations applied to the thermal roughening of vicinal surfaces. In this paper, we will extend the formerly developed diffraction analysis to the case of inhomogeneous vicinal surfaces. First, we consider alternating kinds of terraces [cf. *A* and *B* terraces of Si(001) or Ge(001)]. Second, the influence of terrace size fluctuations is also taken into account, which has been neglected in our previous report. Third, we study the effect of step meandering on the diffraction experiment. In addition, we will apply our analysis to vicinal Ge(001) surfaces with nonequivalent *A* and *B* terraces, which appear due to alternating compressive stress and tensile stress on adjacent terraces. Finally, we will discuss our model in the context of other reports on diffraction from vicinal surfaces.

II. THEORY

A. Basics

Vicinal surfaces consist of terraces which form "staircases." In the following, we assume that the staircase ascends in the (positive) x direction and that the terraces are separated by monatomic steps with step height d. In the following, $R_{n,m}$ denotes the position of the ascending step which confines the nth terrace for the positive x direction (see Fig. 1 for a cross section). The descending step of the nth terrace in the negative x direction is denoted by $R_{n-1,m}$. Of course, the latter step is the ascending step of the $(n-1)$th terrace.

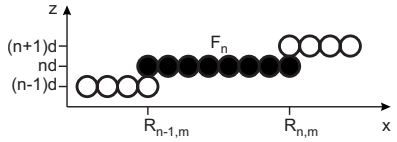

FIG. 1. Schematic drawing of a cross section of a vicinal surface, which ascends in the positive x direction to clarify the nomenclature. The mth row is presented. The nth terrace (emphasized by dark dots) at height $z=nd$ is confined by the ascending step at position $R_{n,m}$ and the descending step at position $R_{n-1,m}$.

The height of the nth terraces is nd. The additional index m denotes the y dependence of the fluctuating position of the nth step in the y direction (see below).

For a vicinal surface, the diffracted wave is described by

$$\Psi(\vec{K}) = \sum_{n,m} F_n \frac{e^{iK_x R_{n-1,m}} - e^{iK_x R_{n,m}}}{1 - e^{iK_x a}} e^{iK_y am} e^{iK_z dn}. \quad (1)$$

Here, K_x, K_y, and K_z denote the x, y, and z component of the scattering vector $\vec{K}=\vec{k}_f-\vec{k}_i$, where $\vec{k}_i$ and $\vec{k}_f$ are the wave vectors of the incoming beam and the diffracted beam, respectively. a and d denote the lateral lattice constant and the vertical lattice constant (step height, see above). For reasons of simplicity, we assume that the unit cells of the terraces have square symmetry so that we can use a Cartesian coordinate system. Surfaces of other symmetries do not influence the following considerations concerning diffraction peak *profiles* but the peak *positions*.

In Eq. (1), F_n is the form factor of the "surface atoms" of the nth terrace. Since most of the surface sensitive diffraction techniques probe not only the atoms of the surface layer but also atoms of layers below the surface (depending on the penetration depth), the form factor includes the scattering by these atoms and multiple scattering effects which are important for electron diffraction (column approximation).[27]

Diffraction techniques do not directly measure the amplitude and phase of the wave $\Psi(\vec{K})$ of the diffracted wave but its intensity $I(\vec{K})=|\Psi(\vec{K})|^2$. For reasons of simplicity, we assume that all surface atoms (more accurately speaking, all columns) have the same form factor F. In principle, the effect of different form factors F can be included in the calculation. The results, however, are very complicated for intensities of diffraction peaks, while the analysis of diffraction spot profiles is not affected. Therefore, form factor effects are beyond the scope of this report. The intensity of the diffracted beam,

$$I(\vec{K}) = |F|^2 G(\vec{K}), \quad (2)$$

separates into the modulus square of the form factor and the lattice factor

$$G(\vec{K}) = \left| \sum_{n,m} \frac{e^{iK_x R_{n-1,m}} - e^{iK_x R_{n,m}}}{1 - e^{iK_x a}} e^{iK_y am} e^{iK_z dn} \right|^2. \quad (3)$$

It is convenient to separate the fluctuating position of the nth step, $R_{n,m}$, into the *average* position R_n and the pure fluctuating part $u_{n,m}$ with $\langle u_{n,m} \rangle_m = 0$, namely,

$$R_{n,m} = R_n + u_{n,m}. \tag{4}$$

Herewith, one obtains the lattice factor

$$G(\vec{K}) = \frac{1-\cos(K_z d)}{1-\cos(K_x a)} \sum_n \langle \rho_{n+n',n'}(K_x) \phi_{n+n',n'}(K_x,K_y) \rangle_{n'} e^{iK_z dn}, \tag{5}$$

with

$$\rho_{n+n',n'}(K_x) = e^{iK_x(R_{n+n'}-R_{n'})} \tag{6}$$

and

$$\phi_{n+n',n'}(K_x,K_y) = \sum_m \langle e^{iK_x(u_{n+n',m+m'}-u_{n',m'})} \rangle_{m'} e^{iK_y am}. \tag{7}$$

Here, the brackets $\langle \cdots \rangle_{m'}$ denote averaging with respect to m'.

Furthermore, we assume that correlations of fluctuations between adjacent steps are negligible. This assumption is reasonable if the average distance between steps (average terrace size) is much larger than the step fluctuations. Correlations of fluctuations, however, may exist for step atoms of the same step due to the stiffness of steps. Therefore, if $n \neq 0$, the averaging with respect to m' in Eq. (7) can be rearranged to

$$\langle e^{iK_x(u_{n+n',m+m'}-u_{n',m'})} \rangle_{m'} = \beta_{n+n'}(K_x) \beta^*_{n'}(K_x), \tag{8}$$

with the characteristic function (Fourier transform) of the step fluctuation distribution

$$\beta_n(K_x) = \langle e^{iK_x u_{n,m'}} \rangle_{m'} = \sum_u P_n(u) e^{iK_x u}. \tag{9}$$

Here, $P_n(u)$ denotes the probability that the fluctuation of the nth step has the value u.

Although we had to assume $n \neq 0$ here to obtain Eq. (8), this result can be extended to the case of $n=0$. Following the considerations of Pukite *et al.*[28] for fluctuations of one dimensional surfaces, for this case ($n=0$), the averaging part of Eq. (7) is

$$\langle e^{iK_x(u_{n,m+m'}-u_{n,m'})} \rangle_{m'} = \sum_{u,u'} P_n(u+u') P_n(u') e^{iK_x u} + \sum_{u,u'} P_n(u+u') P_n(u') \varphi_{n,m}(u) [1 - e^{iK_x u}]. \tag{10}$$

The functions $\varphi_{n,m}(u)$ introduced in Eq. (10) depend on the details of the correlations of the fluctuations (e.g., distribution of kink-kink distances). These details are not important at this point. They will be discussed in more detail in Sec. II C. Despite the ambiguity of the functions $\varphi_{n,m}(u)$, the values of these functions are fixed for two points, namely, the boundary conditions $\varphi_{n,0}(u)=1$ and $\varphi_{n,m}(u)=0$ for $m \to \infty$.

Inserting Eqs. (8) and (10) into Eq. (7), one obtains

$$\phi_{n+n',n'}(K_x,K_y) = \beta_{n+n'}(K_x) \beta^*_{n'}(K_x) \Delta(K_y) + \delta_{n,0} \sum_m \sum_{u'} P_{n'}(u+u') P_{n'}(u') \varphi_{n,m}(u) e^{iK_y am}, \tag{11}$$

with Poisson function

$$\Delta(K_y) = \sum_{n_y} \delta\left(K_y - \frac{2\pi}{a} n_y\right). \tag{12}$$

Here, $\delta(K_y)$ and $\delta_{n,n'}$ denote the delta function and the Kronecker delta, respectively. On the one hand, the second part of Eq. (11) describes the diffuse scattering, which will be discussed later. On the other hand, the first part of Eq. (11) only contributes intensity if $K_y = \frac{2\pi}{a} n_y$, which is one of the lateral Laue conditions of surface diffraction. This part will be discussed here in more detail since it leads to the well-known splitting of diffraction spots due to the vicinality of the surface.

In the following, we assume the lateral Laue condition of zero order ($K_y=0$). Therefore, only the first Brillouin zone is considered. The result, however, can be easily applied to Brillouin zones of higher order if one adds reciprocal lattice vectors.

Under these conditions, Eq. (5) is

$$G(\vec{K}) = \frac{1-\cos(K_z d)}{1-\cos(K_x a)} \times \sum_n \langle \rho_{n+n',n'}(K_x) \beta_{n+n'}(K_x) \beta^*_{n'}(K_x) \rangle_{n'} e^{iK_z dn}. \tag{13}$$

If we further specify the conditions to the case of two alternating types of terraces and steps, named A and B, Eq. (13) can be rearranged to

$$G(\vec{K}) = \frac{1-\cos(K_z d)}{1-\cos(K_x a)} \sum_{X,Y=A}^{B} \beta_X(K_x) \beta^*_Y(K_x) \Phi_{XY}(K_x), \tag{14}$$

where X and Y can be both A or B depending on whether the pair of terraces which interferes are of type A-A or B-B [both terraces must be separated by an odd number of terraces; n of Eq. (13) is even] or A-B or B-A [both terraces must be separated by an even number of terraces; n of Eq. (13) is odd]. Therefore, four summands contribute to the lattice factor. The phase correlation $\Phi_{XY}(K_x)$ is defined via

$$\Phi_{XY}(K_x) = \sum_n \langle \rho^{XY}_{n+n',n'}(K_x) \rangle_{n'} e^{iK_z dn}, \tag{15}$$

where $\rho^{XY}_{n+n',n'}(K_x)$ is defined via Eq. (6) in the way that only terraces of types X and Y, respectively, are considered. Therefore, as mentioned before, n is even if both X and Y are of the same type while n is odd if X and Y are of opposite type.

Further simplifications can be obtained if we assume that the sizes of adjacent terraces are *not* correlated, which is well established in diffraction profile analysis.[28–31] Thus, the phase correlations, which enter Eq. (14), are

$$\Phi_{AA} = \Phi_{BB} = \frac{1}{2}\left(\frac{1+\gamma_A\gamma_B e^{-2iK_z d}}{1-\gamma_A\gamma_B e^{-2iK_z d}} + \text{c.c.}\right),$$

$$\Phi_{AB} = \Phi_{BA}^{*} = \frac{1}{2}\left(\frac{\gamma_B e^{iK_z d}}{1-\gamma_A\gamma_B e^{-2iK_z d}} + \frac{\gamma_A^{*} e^{-iK_z d}}{1-\gamma_A^{*}\gamma_B^{*} e^{2iK_z d}}\right), \tag{16}$$

where γ_A and γ_B denote the Fourier transforms (characteristic functions) of the terrace size distributions $P_A(\Gamma)$ and $P_B(\Gamma)$ of A terraces and B terraces, respectively.

B. Vicinal surfaces with straight steps

Equation (14) describes the general case of alternating types of terraces. However, it is still rather complicated. Therefore, first, we consider straight steps without fluctuations so that $\beta_A(K_x)=\beta_B(K_x)\equiv 1$. In addition, it is assumed that the terrace size distributions of both A terraces and B terraces are well peaked. Therefore, both characteristic functions γ_A and γ_B can be approximated by the second order cumulant approximation[31]

$$\gamma_{A,B} = \exp\left(iK_x\Gamma_{A,B} - \frac{1}{2}K_x^2\sigma_{A,B}^2\right). \tag{17}$$

Here, Γ_A and Γ_B denote the *average* terrace size of A and B terraces, respectively. σ_A and σ_B denote the standard deviations of the terrace size distributions. It should be noted that Eq. (17) is exact for Gaussian distributions and a good approximation for well peaked distributions ($\sigma_{A,B} \ll \Gamma_{A,B}$, see Ref. 31).

Inserting Eq. (17) into Eq. (14) yields

$$\frac{1-\cos(K_x a)}{1-\cos(K_z d)}G(\vec{K}) = 2\frac{\sinh\left[\frac{K_x^2}{2}(\sigma_A^2+\sigma_B^2)\right] + \sinh\left(\frac{K_x^2}{2}\sigma_A^2\right)\cos(K_x\Gamma_B + K_z d) + \sinh\left(\frac{K_x^2}{2}\sigma_B^2\right)\cos(K_x\Gamma_A + K_z d)}{\cosh\left[\frac{K_x^2}{2}(\sigma_A^2+\sigma_B^2)\right] - \cos[K_x(\Gamma_A+\Gamma_B) + 2K_z d]}. \tag{18}$$

Further simplifications can be obtained if the inverse lattice factor $G^{-1}(\vec{K})$ is developed as Taylor approximation of second order with respect to K_x to describe the peak profile as Lorentzian:

$$G(\vec{K}) = \frac{G_0(K_0)}{\kappa^2(K_0) + (K_x - K_0)^2}, \tag{19}$$

with phase dependent peak position

$$K_0 = K_0(K_z) = 2\frac{\pi\nu - K_z d}{\Gamma_A + \Gamma_B}, \tag{20}$$

where ν denotes the order of the diffraction peak with respect to the periodicity $\Gamma_A+\Gamma_B$ of the vicinal surface. Further, the half-width is

$$\kappa(K_0) = \frac{1}{2}\frac{\sigma_A^2+\sigma_B^2}{\Gamma_A+\Gamma_B}K_0^2, \tag{21}$$

and the peak "intensity" is given by

$$G_0(K_0) = 4\frac{1-\cos(K_z d)}{a^2(\Gamma_A+\Gamma_B)^2}[(\sigma_A^2+\sigma_B^2) + \sigma_A^2\cos(K_0\Gamma_B + K_z d) + \sigma_B^2\cos(K_0\Gamma_A + K_z d)]. \tag{22}$$

Equations (20)–(22) are valid if K_0 is in the first Brillouin zone ($|K_0| \leqslant \pi/a$). If higher order spots are considered, K_0 denotes the *deviation* from the lateral Bragg conditions $K_x = 2\pi n_x/a$.

Equation (20) predicts that the position of the diffraction peaks shifts linearly with vertical scattering vector K_z. This is expected also for regularly stepped vicinal surfaces without disorder and with perfect periodicity $\Gamma_A+\Gamma_B$. The diffraction peaks are delta functions for well ordered vicinal surfaces (see Refs. 21 and 22). For disordered vicinal surfaces, however, Eq. (21) shows that the half-width of the peaks varies quadratically with the peak position. Therefore, the peaks become broader and broader the more their positions deviate from the Bragg conditions of the nonvicinal surface ($K_x = 2\pi n_x/a$). The broadening also depends on the standard deviations σ_A and σ_B, respectively. Therefore, it is possible to characterize the terrace size distributions (average terrace size and standard deviation) from recording diffraction peaks at various scattering conditions. This will be demonstrated in the following.

The open dots of Fig. 2 show the diffracted intensity which is exactly calculated from Eq. (14) if the distribution of terrace sizes is governed by gamma distributions

$$P_{A,B}(\Gamma) \propto \left(\frac{M_{A,B}\Gamma}{\Gamma_{A,B}}\right)^{M_{A,B}-1}\exp\left(-\frac{M_{A,B}\Gamma}{\Gamma_{A,B}}\right), \tag{23}$$

with $M_{A,B}=(\Gamma_{A,B}/\sigma_{A,B})^2$. The solid lines of Fig. 2 show Lorentzians which are best fitted to the diffracted intensity peaks [see Eq. (19)]. Obviously, the diffraction peaks are described well by Lorentzians.

The lowest curve is calculated for scattering phase $S=K_z d/2\pi=0.05$. Therefore, the peak of zero order is the strong peak at the center (of the Brillouin zone). The other

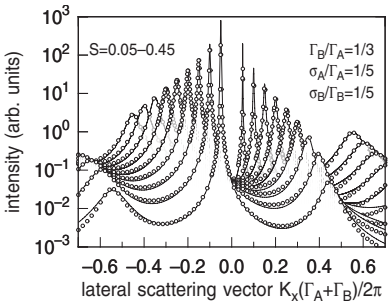

FIG. 2. Phase dependence of the diffraction pattern. Open circles: diffraction intensity calculated from Eq. (14) for $\beta_A=\beta_B=0$ (no step roughness). Solid lines: best fitting of the sum of Lorentzians to the diffraction intensities. Gamma distributions are assumed for the terrace size distribution. The average size of the terraces of type A is three times larger than the average size of the terraces of type B ($\Gamma_B/\Gamma_A=1/3$). The standard deviations of both distributions of A-type terraces and B-type terraces are $\sigma_A/\Gamma_A=\sigma_B/\Gamma_B=1/5$ of the average terrace size. The first line scan is for $S=0.05$ and the last for $S=0.45$. The first line scan shows diffraction peaks of orders $\nu=-1$, $\nu=0$, and $\nu=1$ (from left to right). For higher scattering conditions S, the second order peak ($\nu=2$) appears on the right side.

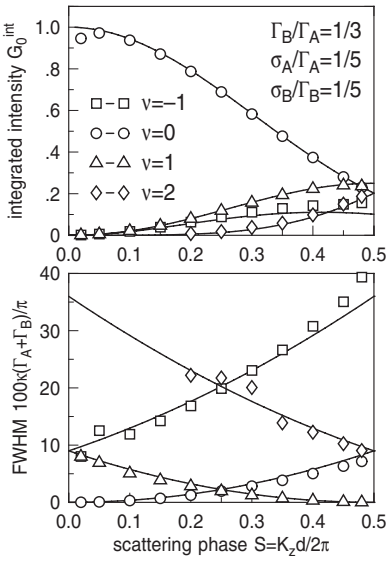

FIG. 3. Phase dependence of the diffraction peaks. Open symbols: parameters obtained from fitting peak profiles to Lorentzians (see Fig. 2). Top: integrated intensities of the peaks ($G_0^{int}=2\kappa G_0$). The solid lines show the behavior obtained from Eq. (24). Bottom: full width at half maximum (FWHM$=2\kappa$). The solid lines show the quadratic behavior as received from Eq. (21).

peaks of this curve are due to (positive and negative) first order. By increasing the phase S, all peaks shift to the left due to the inclination of the vicinal surface. Therefore, another peak appears at the right side of the figure. This peak is the second order diffraction peak.

At once, it is clear that the intensity of the peak of zero order decreases with increasing phase while its half-width increases. The behavior of the peak of (positive) first order, which moves toward the center of the Brillouin zone, is the opposite. Its intensity increases and its half-width decreases since its position moves toward $K_x=0$.

More insight is obtained if the peaks are fitted to Lorentzians. Figure 3 presents the fitted parameters (open symbols) which are the integrated peak intensity and the full width at half maximum (FWHM). For the FWHM (bottom of Fig. 3), the solid lines show the quadratic dependence predicted by Eq. (21). The *integrated* intensity (top of Fig. 3) can be described well by

$$G_0^{int}=2\kappa G_0 \simeq \frac{1-\cos(K_zd)}{1-\cos(K_xa)}[2+\cos(K_x\Gamma_A+K_zd)+\cos(K_x\Gamma_B+K_zd)], \tag{24}$$

which is identical to the intensity from regularly stepped vicinal surfaces. In addition, the linear dependence of the peak position on the scattering phase (not presented here) can be verified from the data, too. Deviations from this behavior, however, can be observed if the terrace size distribution becomes very broad due to higher order components of the characteristic functions γ_A and γ_B (not shown here, see Ref. 31 for nonvicinal surfaces).

On the one hand, Eq. (24) shows that for in-phase conditions, where $S=S_{in}$ is an integer (equivalent to the "Bragg condition" $K_zd=2\pi S_{in}$), the intensity of the lattice factor vanishes for all peaks except the peak which crosses the (nonvicinal) Bragg rod ($K_x=0$, first Brillouin zone). The nonvanishing peak has even order $\nu=2S_{in}$. The integrated intensity of the lattice factor has to equal 1 since the intensity of the lattice factor integrated over one Brillouin zone equals 1.[32] On the other hand, the intensity of all peaks does not vanish for the out-of-phase conditions $S_{out}=S_{in}+\frac{1}{2}$. Here, a peak of odd order ($\nu=2S_{in}+1$) crosses the (nonvicinal) Bragg rod. This peak has the integrated intensity

$$G_0^{int}=\left(\frac{\Gamma_A-\Gamma_B}{\Gamma_A+\Gamma_B}\right)^2. \tag{25}$$

The well-known behavior of homogeneous vicinal surfaces is regained from Eq. (25) since this peak vanishes for homogeneous vicinal surfaces ($\Gamma_A=\Gamma_B$).

Equation (21) predicts a quadratic behavior of the peak width not only with respect to the vertical scattering vector K_z but also with respect to both standard deviations σ_A and σ_B. Figure 4 presents diffraction intensity for $S=0.25$ if the standard deviation σ_A is changed while σ_B is kept constant. Following Eqs. (20)–(22), both the peak of zero order and the peak of first order have equal distance to the center of the Brillouin zone and the same half-width. The intensity of both peaks, however, differs under these scattering conditions [see Fig. 3 (top) for $S=0.25$].

The dots in Fig. 4 show the diffracted intensity which is exactly calculated from Eq. (14) for surfaces without fluctuating steps. The solid lines are best fits of Lorentzians to the diffracted intensity. The agreement is excellent except for very small standard variations (see curve for $\sigma_A/\Gamma_A=1/15$). Both peaks become broader with increasing standard deviation σ_A while the peak intensity decreases. The integrated peak intensity, however, is almost constant, as Fig. 5 demon-

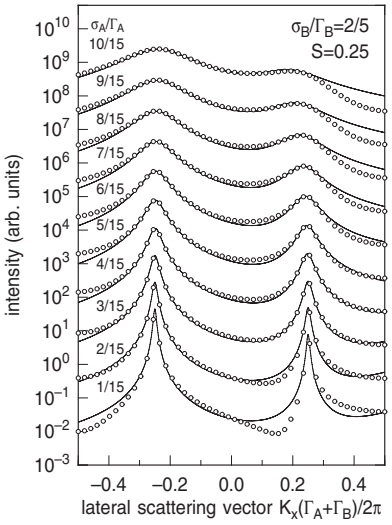

FIG. 4. Roughness dependence of the diffraction pattern for diffraction condition $S=1/4$. Open circles: diffraction intensity calculated from Eq. (14) for $\beta_A=\beta_B=0$ (no step roughness). A logarithmic scale is used because of the large dynamic range of the diffraction intensity. In addition, the line scans are rescaled for reasons of clarity. Solid lines: best fitting of the sum of Lorentzians to the diffraction pattern. Gamma distributions are assumed for the terrace size distribution. The average size of the terraces of type A is three times larger than the average size of the terraces of type B. The standard deviation of the distribution of A-type terraces varies from $\sigma_A/\Gamma_A=1/15$ (bottom) to $\sigma_A/\Gamma_A=10/15$ (top). The standard deviation of B-type terraces is kept constant at $\sigma_B/\Gamma_B=2/5$.

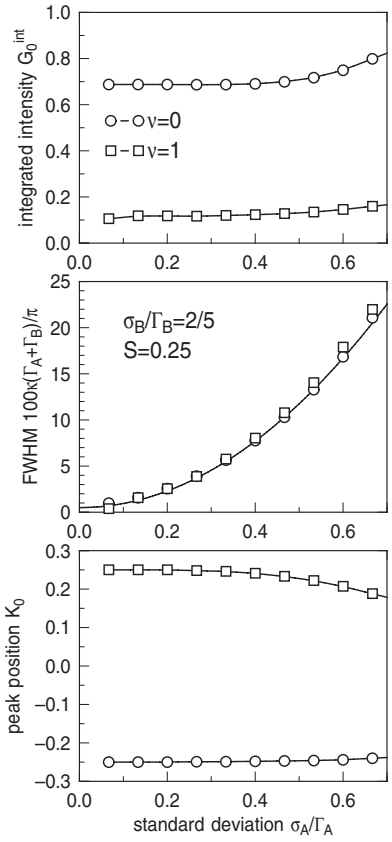

FIG. 5. Roughness dependence of the diffraction peaks. Open symbols: analysis of the Lorentzians of Fig. 4. Top: integrated intensity ($G_0^{int}=2\kappa G_0$) of the peaks, which is almost constant. Center: full width at half maximum (FWHM$=2\kappa$), which follows the quadratic behavior of Eq. (21). The FWHM of the peaks is almost identical due to the symmetry of the diffraction condition. Bottom: peak positions which are almost constant except for large values of the standard deviations σ_A/Γ_A due to higher order effect of the cumulant approximation.

strates. In addition, Fig. 5 proves the quadratic dependence of the FWHM of the peaks on the standard deviation σ_A. The FWHM of both peaks is equal, as Eq. (21) predicts for these scattering conditions. Finally, both peaks shift slightly to the center of the Brillouin zone for very large standard deviations σ_A (see Ref. 31 for peak splitting of diffraction from nonvicinal surface at the out-of-phase condition). This latter behavior is not described by Eq. (20) since higher order components of the characteristic function γ_A are responsible for this behavior.

Finally, the diffraction peak analysis for vicinal surfaces without fluctuating steps can be summarized as follows. On one hand, the average size Γ_A and Γ_B of both terraces of type A and terraces of type B, respectively, can be obtained from the distance between the diffraction peaks and from the residual (scaled) intensity of the peak at out-of-phase condition which is at the nonvicinal Bragg condition (peak of odd order). On the other hand, the *combined* standard variance $\sigma_A^2+\sigma_B^2$ can be obtained from the phase dependence of the FWHM of the peaks. Additional scaling arguments have to be assumed to extract separately the standard deviations σ_A and σ_B. Here, one typical scaling argument may be $\sigma_A/\Gamma_A=\sigma_B/\Gamma_B$. This scaling will be used for the analysis of diffraction patterns obtained from vicinal Ge(001), as presented below.

C. Influence of step meandering

Up to now, it has been assumed that the steps are straight and do not show any fluctuations. Here, we would like to extend the diffraction peak analysis with respect to additional meandering of steps. Following the steps of calculations for the diffraction condition $K_y=2\pi n_y/a$, which led from Eq. (14) to the peak analysis of Eqs. (19)–(22) for vicinal surfaces *without* fluctuating steps, one recovers Eqs. (19)–(21) also for vicinal surfaces *with* fluctuating steps. Equation (22), however, has to be modified:

$$G_0(K_0) = 2\frac{1-\cos(K_z d)}{a^2(\Gamma_A+\Gamma_B)^2}\{(\beta_A^2+\beta_B^2)(\sigma_A^2+\sigma_B^2) + 2\beta_A\beta_B[\sigma_A^2\cos(K_0\Gamma_B+K_z d) + \sigma_B^2\cos(K_0\Gamma_A+K_z d)]\}. \quad (26)$$

Here, we assumed that the distribution of step fluctuations is symmetric so that their characteristic functions $\beta_A(K_x)$ and $\beta_B(K_x)$ are real functions, e.g., Gaussians. Therefore, it is expected that step fluctuations decrease the intensity of the diffraction peaks if their position is not at nonvicinal Bragg conditions ($K_x\neq 2\pi n_x/a$). The peak profiles, however, are not influenced by fluctuations. Therefore, this may be called a static Debye-Waller factor.[33]

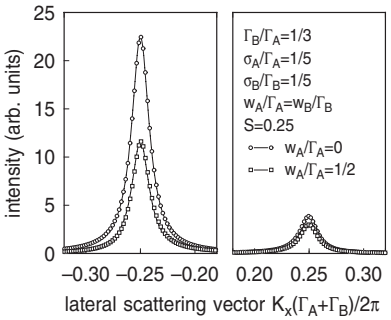

FIG. 6. Influence of the step fluctuations on the diffraction pattern. Open symbols: diffraction intensity calculated from Eq. (14) for scattering phase $S=0.25$ with $\Gamma_B/\Gamma_A=1/3$ and $\sigma_A/\Gamma_A=\sigma_B/\Gamma_B=1/5$. Gamma distributions are assumed for the terrace size distribution. Open dots: no step fluctuations ($w_A=w_B=0$). Open squares: with step fluctuations $w_A/\Gamma_A=w_B/\Gamma_B=1/2$. Solid lines: best fitting of the peaks with Lorentzians. The peak profiles are not affected by step fluctuations but by the intensity of the peaks. Please note that a linear scale is used for the intensity in contrast to the logarithmic scale of previous figures of diffracted intensities.

Figure 6 presents diffraction peaks of zero order and of first order for $S=0.25$ with and without step fluctuations. Please note the linear scale of the intensity. It has been assumed that the distributions of the step fluctuations β_A and β_B are Gaussians while the terrace size distributions follow gamma distributions. Obviously, as expected, the main difference between both sets of peaks is the intensity while the position and the half-width of the peaks do not depend on the step fluctuations.

A detailed study has been performed on diffraction peaks calculated for $S=0.25$ varying the step roughness $w_A=\sqrt{\langle u_A^2\rangle}$ and $w_B=\sqrt{\langle u_B^2\rangle}$ of both types of steps, A and B, while the terrace size distributions are kept constant. It has been additionally supposed that the step roughness scales with the average terrace width of both types of terraces ($w_A/\Gamma_A=w_B/\Gamma_B$) for reasons of simplicity. The analysis of the diffraction peaks is presented in Fig. 7. On the one hand, both the FWHM and the position of the peaks are constant if the step roughness is increased. The integrated intensity, however, decreases with increasing step roughness. The solid lines demonstrate that the attenuation of the peak intensity is described well by Gaussians although the Gaussian form is only exact if the fluctuation of both types of steps is identical [$w_A=w_B$, see Eq. (26)].

If step fluctuations decrease the intensity of the peaks for the lateral Bragg conditions $K_y=2\pi n_y/a$, this intensity has to appear somewhere else in the Brillouin zone since the entire diffracted intensity within one Brillouin zone is independent of the surface morphology.[32] Therefore, the loss of peak intensity is compensated by the intensity due to diffuse diffraction.

The diffuse scattering $G_{diff}(\vec{K})$ for diffraction from homogeneous vicinal surfaces (A terraces and B terraces are of the same type) with uncorrelated step fluctuations has previously been described by Ref. 26. In this report, it has been assumed that the average terrace width is equal for all terraces. However, since the diffuse scattering is governed only by correlation of step fluctuations within the same step [see Eq. (11)], the former result can be easily extended to the case of two different types of steps discussed here:

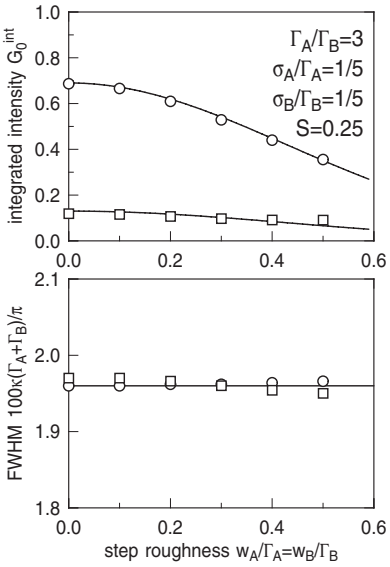

FIG. 7. Influence of the step fluctuations on the diffraction peaks at $S=0.25$, $\Gamma_A/\Gamma_B=3$, and $\sigma_A/\Gamma_A=\sigma_B/\Gamma_B=1/5$. Open symbols: analysis of peak profiles to which Lorentzian profiles are fitted. Top: integrated intensity ($G_0^{int}=2\kappa G_0$) of the peaks, which decreases with increasing amplitude $w_{A,B}$ of the step fluctuations. The solid line shows the Gaussian dependency of the peak intensity on the step fluctuations. Bottom: full width at half maximum (FWHM$=2\kappa$), which is almost constant.

$$G_{diff}(\vec{K}) = G_{diff}^{(A)}(\vec{K}) + G_{diff}^{(B)}(\vec{K}), \tag{27}$$

where $G_{diff}^{(A,B)}(\vec{K})$ are the diffuse lattice factors due to fluctuating steps of type A and fluctuating steps of type B, respectively.

It has been reported that the profile of the diffuse scattering parallel to the steps (K_y direction) has Lorentzian shape if the kink-kink distance is governed by a geometric distribution (noninteracting or weakly interacting kinks).[26] Perpendicular to the steps (K_x direction), it is governed by the characteristic function of the step roughness. This result has to be applied to both parts of the diffuse scattering due to fluctuating steps of type A and of type B. Both parts of the diffuse scattering are described by

$$G_{diff}^{(A,B)}(\vec{K}) = [1-\beta_{A,B}(K_x)]\frac{1-\cos(K_z d)}{1-\cos(K_x a)}\frac{2\kappa_{A,B}(K_x)}{\kappa_{A,B}^2(K_x)+K_y^2}, \tag{28}$$

with

$$\kappa_{A,B}(K_x) = \frac{2w_{A,B}^2}{\xi_{A,B}a^2}\frac{1-\cos(K_x a)}{1-\beta_{A,B}^2(K_x)}. \tag{29}$$

Here, $\xi_{A,B}$ denote the correlation lengths of step fluctuation within steps of type A and of type B, respectively. Therefore, on one hand, the half-widths of both parts of the diffuse

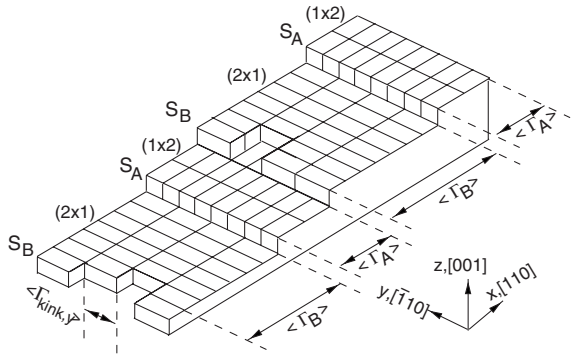

FIG. 8. Model of the vicinal Ge(100) surface with both 1×2 reconstructed A terraces and 2×1 reconstructed B terraces. The terraces are separated by both straight S_A steps and rough S_B steps with different structures due to the different reconstructions of the upper terrace.

scattering close to the Bragg condition $K_x=0$ are governed by $\kappa_{A,B}^{(in)}=\xi_{A,B}^{-1}$. On the other hand, it has been shown for the lateral out-of-phase condition $K_x=\pm\pi/a$ (Brillouin zone boundary) that the half-width is $\kappa_{A,B}^{(out)}=2/\Gamma_{A,B}^{kink}\simeq 4w_{A,B}^2/\xi_{A,B}a^2$. Here, $\Gamma_{A,B}^{kink}$ denote the average kink distances for steps of types A and B, respectively.

Therefore, the parameters (step roughnesses $w_{A,B}$, correlation lengths $\xi_{A,B}$, kink densities) that characterize the step fluctuations can be only obtained from the diffuse diffraction. The step roughness, however, also influences the intensity of the peaks [see Eq. (26)]. Therefore, intensities have to be recalibrated in principle if they are used to characterize the step size distribution [see Sec. II B].

III. EXAMPLE: VICINAL Ge(001)

Here, the diffraction analysis developed in the previous section will be applied to diffraction experiments performed on vicinal Ge(001) surfaces. Surfaces of Ge crystals were prepared with miscuts of 2.7° and 5.4° with respect to the (001) crystal plane and inclined toward the $[\bar{1}\bar{1}0]$ direction, respectively. Details of the preparation of the sample are previously described.[34] Diffraction patterns have been recorded with a high resolution spot profile analysis LEED instrument under ultrahigh vacuum conditions (base pressure of 10^{-8} Pa).

Taking into account the monatomic step height of 1.40 Å and supposing equivalent terraces, the surfaces have average terrace sizes of 29.9 Å and 14.9 Å, respectively, which are equivalent to average terrace sizes of 7.48 and 3.74 lateral lattice constants (a=4.00 Å), respectively. As discussed before, adjacent terraces are not equivalent due to the formation of dimer rows on the (001) surface of Ge, which exist in two 90° rotated domains [see Fig. 8 for a schematic drawing]. Different terraces show either 2×1 or 1×2 reconstruction due to the diamond lattice of Ge. On one hand, A terraces are 1×2 reconstructed where the large side of the unit cell of the superstructure is perpendicular to the descending S_A step. On the other hand, B terraces are 2×1 reconstructed where the large side of the unit cell of the superstructure is parallel to the descending S_B step. The average size Γ_A of A terraces is smaller than the average size Γ_B of B terraces due to the interaction between atomic steps, which is caused by the stress induced by the surface reconstruction. In addition, the different atomic structures of the S_A and S_B steps lead to the formation of rough steps with many kinks (S_A step) and smooth steps with negligible kink formation (S_B step). On the one hand, these prerequisites have to be considered if diffraction patterns from vicinal Ge(001) surfaces are analyzed. On the other hand, we will demonstrate in the following that the analysis of the diffraction pattern may provide detailed data concerning the morphology of such complicated vicinal surfaces as vicinal Ge(001) surfaces (and equivalent surfaces) are.

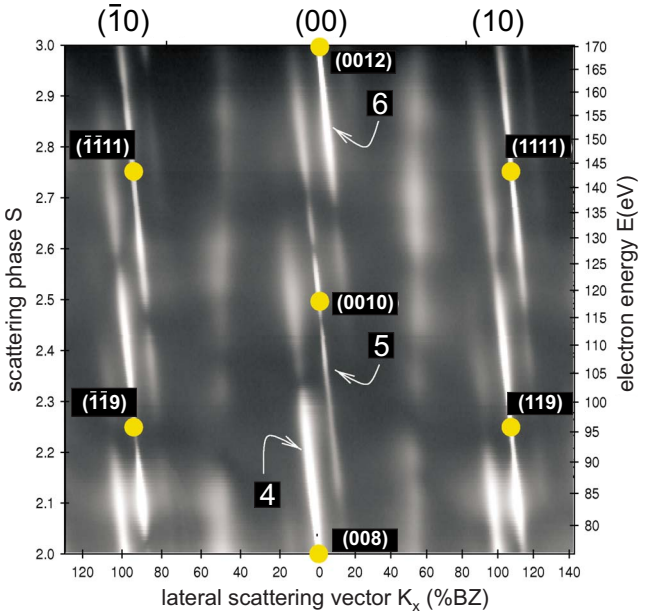

FIG. 9. (Color online) Mapping of the reciprocal space in the plane opened by the vertical [001] vector and the lateral [110] vector. The inclined surface diffraction rods are caused by the 5.4° inclination toward the $[\bar{1}\bar{1}0]$ direction of the surface with respect to the Ge(001) plane. The vertically running rods at $K_x=\pm50\%Bz$ are due to 1×2 reconstructed terraces.

For the sample with miscut of 5.4°, Fig. 9 presents the scattering plane in reciprocal space which is opened by the [110] vector (x direction) and [001] vector (z direction). The figure clearly shows the inclined surface rods due to the vicinality of the surface. These rods run through the Bragg points of three dimensional (3D) diffraction which are denoted with 3D nomenclature, too. For instance, the Bragg points (008) and (0012) denote the second and third in-phase conditions ($S_{in}=2$ and $S_{in}=3$), respectively, of surface diffraction while the out-of-phase condition $S_{out}=2.5$ is denoted by (0010).

In addition, the broad vertical rods at $\pm50\%Bz$ are caused by 1×2 reconstructed A terraces. Here, $\%Bz$ denotes the scaling of the lateral components of scattering vectors K_x and K_y, respectively, to the size of the Brillouin zone ($100\%Bz\equiv2\pi/a$). These rods are also the boundaries of the first Brillouin zone which has been primarily discussed in the previous section.

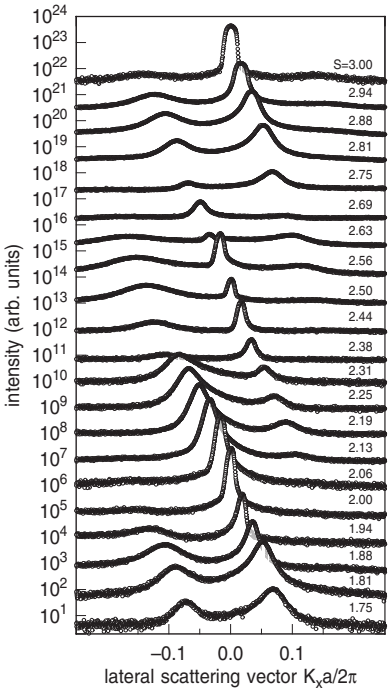

FIG. 10. Diffraction profiles obtained from Ge(001) with 5.4° miscut toward the $[\bar{1}\bar{1}0]$ direction. The profiles are recorded in the direction of miscut. One observes peaks of the orders $\nu=3$ (left peaks) and $\nu=4$ (right peak) for scattering phases below $S=1.75$. The positions of the peaks shift with increasing scattering condition, as expected for vicinal surfaces. Above $S=2$, the peak of order $\nu=3$ vanishes while the peak of order $\nu=5$ appears at the right side. The peak of order $\nu=6$ appears close to $S=2.5$ at the right side.

We will analyze the surface rods due to vicinality in the following. The vertical axis of Fig. 9 runs from the in-phase condition $S=2$ to the in-phase condition $S=3$. Therefore, the inclined diffraction rods visible in the first surface Brillouin zone are of fourth ($\nu=4$) to sixth ($\nu=6$) orders as denoted in Fig. 9. The equivalent points of crossing at $K_x=\pm 100\%Bz$ differ for the surface rods in the adjacent Brillouin zones due to the diamond lattice of the Ge sample. These points are at $S=2.25$ [with 3D nomenclature (119) for the (10) rod and $(\bar{1}\bar{1}9)$ for the $(\bar{1}0)$ rod] and $S=2.75$ [with 3D nomenclature (1111) for the (10) rod and $(\bar{1}\bar{1}11)$ for the $(\bar{1}0)$ rod].

Profiles of the diffraction peaks, which are recorded in the [110] direction, are shown in Fig. 10. It is again obvious that the diffraction peaks shift into the $[\bar{1}\bar{1}0]$ direction with increasing scattering phase S. The influence of the scattering phase on both the intensity and the half-width of the peaks, however, can be better judged here than in Fig. 9. Starting from the bottom of Fig. 10 ($S=1.75$), one sees the diffraction peaks of orders $\nu=3$ (left) and $\nu=4$ (right), respectively. Increasing the scattering phase S, the diffraction peak $\nu=3$ becomes broader and less intense while the diffraction peak $\nu=4$ becomes sharper and more intense. At $S=2$ (in-phase condition), only the diffraction peak $\nu=4$ is visible while the diffraction peak $\nu=3$ vanished. Beyond $S=2$, the diffraction peak $\nu=5$ appears on the right side. First, this peak is broad. However, it sharpens and becomes more intense if the scattering phase S approaches $S=2.5$ (out-of-phase condition). Here, the (broad) diffraction peak $\nu=6$ also appears. Beyond $S=2.5$, the interplay between intensity and half-width of the diffraction peaks depending on the scattering phase S can be observed again.

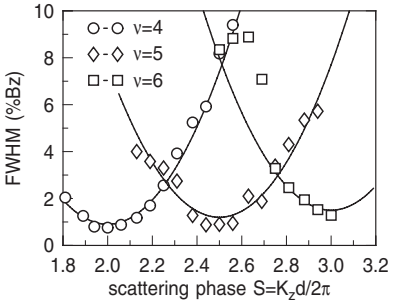

FIG. 11. FWHM of diffraction peaks of orders $\nu=4$, $\nu=5$, and $\nu=6$ obtained from Ge(001) with 5.4° miscut toward the $[\bar{1}\bar{1}0]$ direction. The FWHM of the peaks follows the square dependence predicted by Eq. (21).

This behavior of phase dependent position and half-width of the peaks is in full agreement with the theory developed in this paper. Diffraction peaks are sharp if they cross $K_x=0\%Bz$, while their half-width increases the more the position is shifted from the center of the Brillouin zone [see Eqs. (20) and (21)]. The half-width of the peaks at $K_x=0\%Bz$ is only determined by the instrumental broadening (or other defects as mosaics).

The peak profiles of different diffraction orders have been fitted by Lorentzians to specify the phase dependence of both the intensity and the FWHM on the scattering phase. The result for the FWHM is presented in Fig. 11. The FWHMs of the peaks follow the parabolic dependence predicted by Eq. (21). The combined variance $\sigma_A^2+\sigma_B^2=8.1a^2$ is obtained from the curvature of the phase dependence of the FWHM for the peaks of diffraction orders $\nu=4$ to $\nu=6$. As previously stated, one can only proceed further in analyzing the data if one takes into account an additional condition. We will assume that the terrace size distribution scales with the average terrace size, namely, $\sigma_A/\Gamma_A=\sigma_B/\Gamma_B$.

Therefore, one has to evaluate the average terrace sizes Γ_A and Γ_B, which can be easily obtained from the intensity of the diffraction peaks at the out-of-phase condition.[32] Following Eq. (25), one obtains $\Gamma_A/\Gamma_B=0.35$ for the sample with miscut of 5.4° examined here. Finally, one can evaluate $\Gamma_A=1.94a$ and $\Gamma_B=5.54a$ taking into account the value $\Gamma_A+\Gamma_B=7.48a$ obtained from the distances of the different peaks. Finally, the specific standard deviations $\sigma_A=0.9a$ and $\sigma_B=1.7a$ can be obtained if one supposes a scaling behavior of terrace size distributions.

At this point, we have to mention that we did not take into account the diffuse scattering for the intensity analysis presented above. As discussed in Sec. II C, step roughness decreases the intensity of the diffraction peaks and causes diffuse scattering. The step roughness can be obtained from analyzing the diffuse diffraction intensity (see below). One can estimate a scaled step roughness of $w_B/(\Gamma_A+\Gamma_B)\simeq 0.15$ for the sample of 5.7° miscut. The effect of step roughness on the diffraction peaks $\nu=4$ and $\nu=6$, however, is negli-

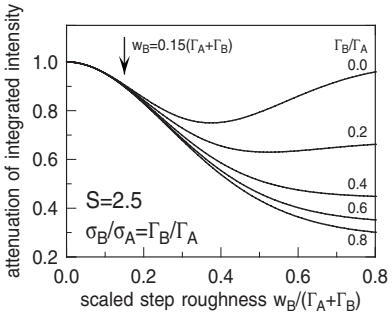

FIG. 12. Attenuation of the intensity of the diffraction peaks of fourth and sixth orders with respect to the step roughness w_B. From diffuse diffraction data, $w_B=0.15(\Gamma_A+\Gamma_B)$ is estimated. Therefore, the attenuation is negligible within the error of the experimental data.

gible, as demonstrated by Fig. 12. The effect on the intensity is less than 10%, yielding an even smaller influence of less than 5% on the scaling quantity Γ_A/Γ_B. Therefore, we do not consider the step roughness for the analysis of the terrace size distribution.

For the sample with miscut of 2.7°, Fig. 13 presents an in-plane scan (K_x-K_y scattering plane) for scattering condition $S=3.7$. Three different diffraction peaks of orders $\nu=7$ to $\nu=9$ can be seen from left to right. While we previously considered profiles of the diffraction peaks in the x direction, here we will analyze the diffuse scattering in the y direction (dashed lines in Fig. 13) to obtain information about the step roughness.

Figure 14(a) presents profiles of the diffuse scattering recorded in the $[\bar{1}10]$ direction (y direction) for different K_x

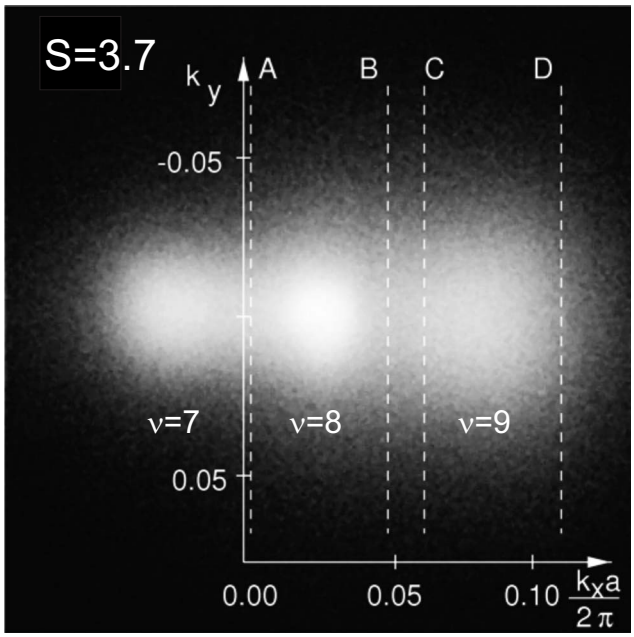

FIG. 13. Two-dimensional diffraction pattern recorded from a vicinal Ge(001) surface with 2.7° miscut toward the $[\bar{1}\bar{1}0]$ direction for scattering phase $S=3.7$. The diffraction peaks are of the orders $\nu=7$ (left) to $\nu=9$ (right). The dashed lines show line scans of the diffuse diffraction presented and analyzed in Fig. 14.

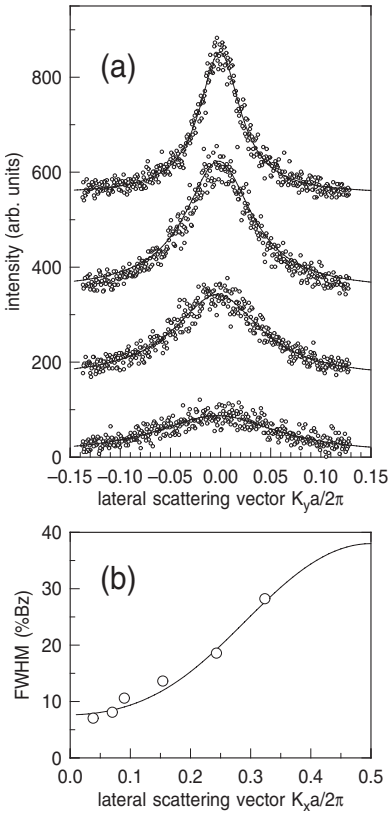

FIG. 14. (a) Line scans extracted from Fig. 13 recorded in the $[\bar{1}10]$ direction (y direction) for different values of K_x. (b) K_x dependence of the FWHM of the line scans. The line shows the dependence described by Eq. (29).

values but constant scattering phase ($S=3.7$). The intensity of the diffuse intensity decreases with increasing K_x while the FWHM of the diffuse scattering increases. This behavior can be attributed to the formation of kinks of meandering steps, as predicted by Eq. (29).

As pointed out in Sec. II C, in principle, one cannot distinguish from the diffraction experiment what the contributions of S_A steps and S_B steps are. For the case of Ge(001), however, the diffuse scattering can be essentially attributed to the kink formation of S_A steps since it is well known from STM experiments that S_B steps rarely form kinks. Therefore, we assumed $w_A=0$ and analyzed the K_x dependence of the FWHM of the diffuse scattering with respect to w_B. Figure 14(b) shows that the K_x dependence can be described well by Eq. (29). Fitting the data, we obtain a correlation length $\xi=4.2a$ (16.6 Å) and a step roughness of $w_B=1.1a$ (4.4 Å). Therefore, the kink-kink distance is $\Gamma_B^{kink}=3.4a$ (13.6 Å) for the S_B steps. In addition, the basic assumption of this report, namely, $w_B \ll \Gamma_A, \Gamma_B$, can be verified *a posteriori*.

IV. DISCUSSION AND SUMMARY

This report deals with the influence of step roughness and terrace size distributions on diffraction experiments performed on (inhomogeneous) vicinal surfaces with alternating terraces. Therefore, the model developed here is adequate to

TABLE I. Overview of surface properties and their influence on the diffraction pattern.

Surface property	Scattering condition	Diffraction property	Equation
Average terrace length $\Gamma_A+\Gamma_B$	Any	Distance ΔK_0 of diffraction peaks	(20)
Ratio of terrace sizes Γ_A/Γ_B	Out-of-phase condition $S=n+\frac{1}{2}$	Intensity ratio G_0^{int} of diffraction peaks	(25)
Standard deviation of terrace size distribution $\sigma_A+\sigma_B$	Variation of S close to Bragg condition	FWHM $2\kappa(S)$ of diffraction peak	(21)
Correlation length ξ_A, B of meandering steps	Diffuse scattering close to Bragg rod	FWHM $2\kappa_{A,B}^{in}$ of diffuse scattering	(29)
Average distance $\Gamma_{A,B}^{kink}$ of kinks	Diffuse scattering close to boundary of Brillouin zone	FWHM $2\kappa_{A,B}^{out}$ of diffuse scattering	(29)
rms width w of meandering steps	Dependence of diffuse scattering on K_x	FWHM $2\kappa_{A,B}(K_x)$ of diffuse scattering	(29)

surfaces such as Si(001) and Ge(001), as well as surfaces of alloys which tend to form paired steps. The analysis of diffraction pattern yields morphologic data such as average terrace sizes, standard deviations of terrace size distributions, as well as correlation lengths, kink densities, and (rms) widths of meandering steps (see Table I). Therefore, the theory may also be applied to diffraction from vicinal surfaces with meandering steps of single height to characterize wavy steps which, for instance, is observed for Si(001) vicinal surfaces with extremely small miscut (less than 0.1°).[35,36] However, we would like to emphasize that one needs diffraction experiments with very high resolution to record diffraction peak profiles as provided by grazing incidence x-ray diffraction (GIXRD).

Previous diffraction studies on Si(001) focused on the asymmetry between the coverage of both A and B terraces which is equivalent to the asymmetry between average terrace sizes Γ_A and Γ_B, respectively. Therefore, asymmetries of intensities of diffraction peaks have been analyzed but not spot profiles of diffraction peaks.

For instance, the ratio of terrace sizes has been evaluated from the asymmetry of the intensity of both 1×2 and 2×1 superstructure peaks of Si(001), which are under external stress.[37,38] The intensity from the 90° rotated domains has been associated with both A and B terraces. Splitting of the superstructure spots into two (or more) peaks due to correlation of the reconstruction of adjacent terraces has been observed for vicinal Si(100) surfaces which are dominated by D_B double steps and B terraces.[39,40] It has been pointed out that short terrace sizes may be underestimated by this method.[41]

Therefore, de Miguel *et al.* analyzed the intensity of the peak at $K_x=0\%Bz$ at the out-of-phase condition with respect to the adjacent peaks in reciprocal space to obtain ratios between average terrace sizes for vicinal Si(001) with different angles of miscut.[41] This procedure accords with Eq. (25). It has been applied by other groups, too.[42] In addition, the peak profiles for different scattering conditions presented (but not discussed) by these authors confirm the diffraction analysis developed here. On one hand, diffraction peaks are sharp if they are close to $K_x=0\%Bz$. On the other hand, the peaks broaden if their position shifts to higher or lower values of K_x.

The diffraction study presented here treats (two dimensional) diffraction from vicinal surfaces with alternating terraces of different average sizes. Information concerning the morphology of these surfaces is obtained from analyzing the profiles of both diffraction peaks and diffuse scattering.

Early reports concerning diffraction spot profile analysis refer to homogeneous vicinal surfaces with equal conditions for every step. Lu and co-workers developed statistical models for one dimensional surfaces which do not consider the influence of step meandering due to the reduced dimensionality.[43,44] Therefore, these studies focused on the influence of terrace size distributions on diffraction peak profiles. For instance, the authors report the splitting into two peaks for the out-of-phase condition if the terrace size distribution is governed by cut-off geometric distributions where terraces of small size are totally suppressed $[P(\Gamma\leqslant\Gamma_0)=0]$. Although one can easily obtain analytic solutions for the calculation of peak profiles, the cut-off geometric distribution is rather nonphysical. Thus, it seems better suited to use the gamma distribution [cf. Eq. (23)] as we do in our model calculations.

Nevertheless, our results comprised in Eqs. (19)–(22) are generally valid and independent of the exact form of the terrace size distribution. Therefore, the results presented by Lu and co-workers qualitatively agree with our results.[43,44] For instance, the peaks become sharper if the terrace size distribution becomes sharper. In addition, the phase dependent FWHM of the peaks has been reported, which is also predicted by Eq. (21).

Furthermore, for the out-of-phase condition, one can compare our result for vicinal surfaces with the diffraction peaks obtained for rough singular (nonvicinal) surfaces (out-of-phase projection of stepped surface on two-level system[32]).

Here, the FWHM of diffraction peaks of even order ν quadratically decreases for decreasing standard deviation at the out-of-phase condition ($K_0=\pm\pi/\langle\Gamma\rangle$ with $\Gamma_A=\Gamma_B=\langle\Gamma\rangle$). This result coincides with former calculations for diffraction peaks at the out-of-phase condition from surfaces with peaked terrace size distribution.[31] Here, we would like to remark that the peaks of odd diffraction order $\nu=2S_{out}$ (peak at $K_x=0$ for out-of-phase condition), which are sharp at the out-of-phase condition, do not appear for homogeneous *vicinal* surfaces due to symmetry $\Gamma_A=\Gamma_B$. However, *singular* surface with nonequal distributions between layers of odd and even heights (scaled to the layer distance d) lead to the remaining central peak intensity (in our model, the diffraction peak of odd order $\nu=2S_{out}$), too.

Later, the effect of step roughness of homogeneous surfaces on the diffraction intensity has been treated for slit integrated intensities with the path of integration perpendicular to the meandering step edge.[45,46] The authors report that diffraction peaks split into a sharp peak and diffuse scattering for the out-of-phase condition. This is in good agreement with the model presented here. After slit integration (x direction), the separated peaks due to the vicinality for $K_y=0$ collapse into one central spike while there exists an additional profile due to the two dimensional distribution of diffuse scattering.

The results of Lagallay and co-workers have been applied to vicinal Si(100).[45,46] The angle of miscut, however, has been 0.2°, which is much smaller than the critical angle for the transition from single layer steps (S_A and S_B) to double layer steps (D_B). Therefore, the asymmetry between A terraces and B terraces is not well developed. This asymmetry has not been taken into account in these studies concerning step roughness.

Based on quadratic model Hamiltonians with different coupling parameters, the same group presented two dimensional calculations for vicinal surfaces, too.[47] Although the calculation of the intensity has been generally done numerically, it can be shown under the assumption of strongly correlated meandering of adjacent steps that the diffuse scattering can be described by the sum of Lorentzians (with respect to K_y). This agrees with Eq. (28) although our model is based on noncorrelated meandering of step edges.

One important physical property of homogeneous vicinal surfaces, which has been under discussion for a long time, is the thermally activated roughening at high temperatures. From terrace-step-kink models (including Monte Carlo simulations), power laws have been predicted for the profiles of diffraction peaks.[48,49] The two dimensional diffraction analysis has been extended to the case of SXRD from vicinal surfaces, where the power laws are regained for transverse profiles.[50,51] The temperature dependence of the exponent has been used to determine the critical temperature for the roughening transition of vicinal surfaces (see Ref. 5 for an overview).

Some authors, however, reported other peak profiles as Lorentzians for the diffuse diffraction from rough vicinal surfaces.[52] Bartelt *et al.* later emphasized the importance of step collisions on both correlation functions and diffraction profiles.[53] The correlation on short length scales (compared to the average distance for step collisions y_{coll}) differs from the behavior on large length scales. Consequently, the power law is only valid for small scattering vectors K_y while Lorentzian peak profiles are observed for large K_y. Since we exclude step collisions in our model, we only observe the Lorentzian behavior for transverse scans parallel to step edges [see Eq. (28)].

The diffraction analysis presented here assumes that effects due to different form factors of both A and B terraces can be neglected. This assumption may be questionable under certain scattering geometries since the different orientations of both 1×2 and 2×1 reconstruction unit cells influence the form factor. For the standard LEED geometry with normal incidence, however, form factor effects can be excluded due to the symmetry of the diffraction experiment. This is not the case for experiments with grazing incidence such as reflection high energy electron diffraction (RHEED) or GIXRD. For instance, it has been reported that diffraction peaks appear, which are forbidden for the kinematic approximation, for diffraction from Si(001) if LEED experiments are performed with non-normal incidence.[54]

Beyond the simple kinematic approximation of the diffraction profile analysis presented here, we investigated the effect of alternating form factor of A terraces and B terraces, too. We did not present the full evaluation of the diffraction pattern since the evaluation is quite complicated except for simple diffraction conditions such as in-phase condition or out-of-phase condition. However, we will shortly discuss the main features we obtained due to the additional effect of different form factors for A terraces and B terraces.

On the one hand, different form factors influence intensities so that intensities cannot be used to determine the morphology of the surface, e.g., differences of the average terrace sizes Γ_A and Γ_B. Therefore, it is not possible to evaluate the coverage of A terraces and B terraces from Eq. (25). This complicates the analysis. On the other hand, the profiles of peaks do not depend on form factor effects so that Eqs. (20) and (21) still hold and can be used to determine statistical parameters such as $\Gamma_A+\Gamma_B$ and $\sigma_A^2+\sigma_B^2$, respectively. The analysis of the step roughness is also not influenced by form factor effects since the dependence of FWHM on K_x is important, but not the intensity.

In addition, we would like to emphasize that form factor effects can be suppressed even for grazing incidence if high symmetry scattering planes are used for the diffraction experiment. For instance, one can use the scattering plane opened by both the [100] direction and the [001] direction for experiments with Si(100) and Ge(100). Under these conditions, both kinds of dimers of A terraces and B terraces are inclined by 45° with respect to the scattering plane so that the form factors are equal.[55]

In summary, we presented a full model for the diffraction from inhomogeneous vicinal surfaces with inequivalent terraces. Therefore, the model is ideal for diffraction from semiconductor surfaces with terrace dependent reconstruction [e.g., Si(001) and Ge(001)], as well as for some surfaces of alloys which tend to form pairs of steps. The analysis is based on the kinematic approximation. Therefore it is valid if profiles of peaks and diffuse diffraction are considered. In addition, *ratios between intensities* of peaks can be analyzed.

We demonstrate that diffraction experiments with adequate analysis provide many important parameters such as average sizes and standard deviations of terrace size distributions, as well as rms widths, correlation lengths, and kink densities of meandering steps, to characterize the morphology of vicinal surfaces. Finally, we applied our model to the analysis of vicinal Ge(001) surfaces with miscut toward the [110] direction.

[1] W. K. Burton, N. Cabrera, and F. C. Frank, Philos. Trans. R. Soc. London, Ser. A **243**, 299 (1951).
[2] I. V. Markov, *Crystal Growth for Beginners* (World Scientific, Singapore, 1995).
[3] M. A. Herman, W. Richter, and H. Sitter, *Epitaxy* (Springer, Berlin, 2004).
[4] G. A. Somorjai, *Introduction to Surface Chemistry and Catalysis* (Wiley, New York, 1994).
[5] J. Lapujoulade, Surf. Sci. Rep. **20**, 195 (1994).
[6] L. Barbier, S. Goapper, B. Salanon, R. Caudron, A. Loiseau, J. Alvarez, S. Ferrer, and X. Torrelles, Phys. Rev. Lett. **78**, 3003 (1997).
[7] E. Le Goff, L. Barbier, S. Goapper, A. Loiseau, and B. Salanon, Surf. Sci. **466**, 73 (2000).
[8] H. J. W. Zandvliet, Rev. Mod. Phys. **72**, 593 (2000).
[9] H. J. W. Zandvliet, Phys. Rep. **388**, 1 (2003).
[10] P. E. Wierenga, J. A. Kubby, and J. E. Griffith, Phys. Rev. Lett. **59**, 2169 (1987).
[11] O. L. Alerhand, D. Vanderbilt, R. D. Meade, and J. D. Joannopoulos, Phys. Rev. Lett. **61**, 1973 (1988).
[12] O. L. Alerhand, A. N. Berker, J. D. Joannopoulos, D. Vanderbilt, R. J. Hamers, and J. E. Demuth, Phys. Rev. Lett. **64**, 2406 (1990).
[13] N. C. Bartelt, T. L. Einstein, and C. Rottman, Phys. Rev. Lett. **66**, 961 (1991).
[14] S. Dey, S. Kiriukhin, J. West, and E. H. Conrad, Phys. Rev. Lett. **77**, 530 (1996).
[15] J. A. Yancey, H. L. Richards, and T. L. Einstein, Surf. Sci. **598**, 78 (2005).
[16] Q. Chen and N. V. Richardson, Prog. Surf. Sci. **73**, 59 (2003).
[17] H. C. Jeong and E. D. Williams, Surf. Sci. Rep. **34**, 171 (1999).
[18] M. Giesen, Prog. Surf. Sci. **68**, 1 (2001).
[19] W. P. Ellis and R. L. Schwoebel, Surf. Sci. **11**, 82 (1968).
[20] M. Henzler, Surf. Sci. **19**, 159 (1970).
[21] M. Henzler, Appl. Phys. **9**, 11 (1976).
[22] M. Henzler, in *Electron Spectroscopy for Surface Analysis*, edited by H. Ibach (Springer, Berlin, 1977), p. 117.
[23] M. Henzler and J. Clabes, in Proceedings of the Second International Conference on Solid Surfaces, 1974 (unpublished); Jpn. J. Appl. Phys., Suppl. **2**, 389 (1974).
[24] B. Z. Olshanetzky and A. A. Shklyaev, Surf. Sci. **82**, 445 (1979).
[25] R. Kaplan, Surf. Sci. **93**, 145 (1980).
[26] J. Wollschläger and M. I. Larsson, Phys. Rev. B **57**, 14937 (1998).
[27] M. Henzler, Appl. Phys. A: Solids Surf. **34**, 205 (1984).
[28] P. R. Pukite, C. S. Lent, and P. I. Cohen, Surf. Sci. **167**, 39 (1985).
[29] S. Pflanz and W. Moritz, Acta Crystallogr., Sect. A: Found. Crystallogr. **48**, 716 (1992).
[30] J. Wollschläger, Surf. Sci. **328**, 325 (1995).
[31] J. Wollschläger, Surf. Sci. **383**, 103 (1997).
[32] M. Henzler, in *RHEED and Reflection Electron Imaging of Surfaces*, edited by P. K. Larsen and P. J. Dobson (Plenum, New York, 1988), p. 193.
[33] D. E. Savage, J. Kleiner, N. Schimke, Y. H. Phand, J. Jacobs, R. Kariotis, and M. G. Lagallay, J. Appl. Phys. **69**, 1411 (1991).
[34] C. Tegenkamp, J. Wollschläger, H. Pfnür, F. J. Meyer zu Heringdorf, and M. Horn-von Hoegen, Phys. Rev. B **65**, 235316 (2002).
[35] R. M. Tromp and M. C. Reuter, Phys. Rev. Lett. **68**, 820 (1992).
[36] R. M. Tromp and M. C. Reuter, Phys. Rev. B **47**, 7598 (1993).
[37] F. K. Men, W. E. Packard, and M. B. Webb, Phys. Rev. Lett. **61**, 2469 (1988).
[38] M. B. Webb, Surf. Sci. **299/300**, 454 (1994).
[39] C. E. Aumann, D. E. Savage, R. Kariotis, and M. G. Lagally, J. Vac. Sci. Technol. A **6**, 1963 (1988).
[40] E. Schröder-Bergen, W. Ranke, and K. Jacobi, Solid State Commun. **71**, 89 (1989).
[41] J. J. de Miguel, C. E. Aumann, R. Kariotis, and M. G. Lagally, Phys. Rev. Lett. **67**, 2830 (1991).
[42] E. Schröder-Bergen and W. Ranke, Surf. Sci. **259**, 323 (1991).
[43] M. Presicci and T. M. Lu, Surf. Sci. **141**, 233 (1984).
[44] J. M. Pimbley and T. M. Lu, Surf. Sci. **159**, 169 (1985).
[45] D. Saloner, J. A. Martin, M. C. Tringides, D. E. Savage, C. E. Aumann, and M. G. Lagally, J. Appl. Phys. **61**, 2884 (1987).
[46] R. Kariotis, B. S. Swartzentruber, and M. G. Lagally, J. Appl. Phys. **67**, 2848 (1990).
[47] J. Kleiner, C. E. Aumann, Y. W. Mo, R. Kariotis, and M. G. Lagally, Surf. Sci. **240**, 293 (1990).
[48] J. Villain, D. R. Grempel, and J. Lapujoulade, J. Phys. F: Met. Phys. **15**, 809 (1985).
[49] N. C. Bartelt, T. L. Einstein, and E. D. Williams, Surf. Sci. **244**, 149 (1991).
[50] D. Y. Noh, K. I. Blum, M. J. Ramstad, and R. J. Birgeneau, Phys. Rev. B **48**, 1612 (1993).
[51] G. A. Held and J. D. Brock, Phys. Rev. B **51**, 7262 (1995).
[52] J. Wollschläger, E. Z. Luo, and M. Henzler, Phys. Rev. B **44**, 13031 (1991).
[53] N. C. Bartelt, T. L. Einstein, and E. D. Williams, Surf. Sci. **276**, 308 (1992).
[54] J. A. Martin, C. E. Aumann, D. E. Savage, M. C. Tringides, M. G. Lagally, W. Moritz, and F. Kretschmar, J. Vac. Sci. Technol. A **5**, 615 (1987).
[55] J. Wollschläger, Diploma thesis, Universität Hannover, 1987.